PNAS RESEARCH ARTICLE | IMMUNOLOGY AND INFLAMMATION

Agonist concentration–dependent changes in FPR1 conformation lead to biased signaling for selective activation of phagocyte functions

Junlin Wang[a] and Richard D. Ye[a,1]

Edited by Jason Cyster, HHMI, University of California, San Francisco, CA; received January 27, 2022; accepted June 17, 2022

The bacteria-derived formyl peptide fMet-Leu-Phe (fMLF) is a potent chemoattractant of phagocytes that induces chemotaxis at subnanomolar concentrations. At higher concentrations, fMLF inhibits chemotaxis while stimulating degranulation and superoxide production, allowing phagocytes to kill invading bacteria. How an agonist activates distinct cellular functions at different concentrations remains unclear. Using a bioluminescence resonance energy transfer–based FPR1 biosensor, we found that fMLF at subnanomolar and micromolar concentrations induced distinct conformational changes in FPR1, a Gi-coupled chemoattractant receptor that activates various phagocyte functions. Neutrophil-like HL-60 cells exposed to subnanomolar concentrations of fMLF polarized rapidly and migrated along a chemoattractant concentration gradient. These cells also developed an intracellular Ca^{2+} concentration gradient. In comparison, high nanomolar and micromolar concentrations of fMLF triggered the PLC-β/diacyl glycerol/inositol trisphosphate pathway downstream of the heterotrimeric Gi proteins, leading to Ca^{2+} mobilization from intracellular stores and Ca^{2+} influx from extracellular milieu. A robust and uniform rise in cytoplasmic Ca^{2+} level was required for degranulation and superoxide production but disrupted cytoplasmic Ca^{2+} concentration gradient and inhibited chemotaxis. In addition, elevated ERK1/2 phosphorylation and β-arrestin2 membrane translocation were associated with diminished chemotaxis in the presence of fMLF above 1 nM. These findings suggest a mechanism for FPR1 agonist concentration–dependent signaling that leads to a switch from migration to bactericidal activities in phagocytes.

GPCRs | biased signaling | phagocytes | calcium mobilization

Significance

The present study reports biased signaling of a G protein-coupled receptor (GPCR) in a ligand concentration–dependent manner, in contrast to ligand-specific biased signaling in many GPCRs. Using FPR1, a class A GPCR, this study demonstrates the presence of distinct receptor conformations induced by low and high concentrations of the bacterial agonist *N*-formyl-Met-Leu-Phe, with a corresponding switch of phagocyte functions from chemotaxis to degranulation and superoxide production. These findings suggest that distinct phagocyte functions may be activated by biased signaling through a GPCR exposed to different concentrations of the same agonist, thus providing a mechanism that may expand the scope of research on GPCR signaling.

The formyl peptide receptors (FPRs) are G protein–coupled receptors (GPCRs) expressed mainly in phagocytes and mediate migratory and bactericidal functions, including chemotaxis, degranulation, and superoxide production. To date, three FPR genes have been identified in humans that encode FPR1, FPR2 and FPR3, respectively (1). FPR1, one of the first cloned human chemoattractant receptors (2), recognizes short peptides bearing *N*-formyl-Met from bacteria and mitochondria as pathogen- and damage-associated molecular patterns, respectively. The prototypic formyl peptide from *Escherichia coli*, *N*-formyl-Met-Leu-Phe (fMLF), is the shortest full agonist of FPR1 (3) and is widely considered a key chemoattractant for directional migration of phagocytes to the site of bacterial infection (4, 5). Accumulation of phagocytes such as neutrophils in inflammatory tissues not only helps to eliminate invading bacteria but also contributes to inflammatory responses that may cause damage to tissues and organs. Precise regulation of phagocyte activation, therefore, is highly important for host defense as well as resolution of inflammation. To this end, research has been carried out in the studies of endogenous factors serving to resolve inflammation through FPR2, one of the formyl peptide receptors (1, 6).

FPR1, like other chemoattractant receptors, is functionally coupled to the Gi class of heterotrimeric G proteins (7). All phagocyte functions induced by FPR1, including chemotaxis, degranulation, and superoxide generation, require Gi coupling (8). It has been well recognized that FPR1 ligands such as fMLF can induce phagocyte chemotaxis at picomolar to low nanomolar concentrations. However, at higher nanomolar and micromolar concentrations, fMLF preferentially stimulates phagocyte degranulation and superoxide generation while suppressing chemotaxis. The concentration-dependent activation profile suits innate immunity very well: It helps to avoid unwanted tissue damage en route to the infection site but enhances the release of granule contents and superoxide following phagocytosis of the invading bacteria at sites of infection (4, 9). How phagocytes respond to different concentrations of chemoattractants with selective activation of cellular functions remains unclear. Early studies have shown that FPR1 combined with the necessary signaling molecules and effector proteins (e.g., NOX2) could be sufficient to reconstitute degranulation and

Author affiliations: [a]Kobilka Institute of Innovative Drug Discovery and School of Life and Health Sciences, School of Medicine, The Chinese University of Hong Kong, Shenzhen, Guangdong 518172, China

Author contributions: J.W. and R.D.Y. designed research; J.W. performed research; J.W. analyzed data; and J.W. and R.D.Y. wrote the paper.

The authors declare no competing interest.

This article is a PNAS Direct Submission.

[1]To whom correspondence may be addressed. Email: richardye@cuhk.edu.cn.

This article contains supporting information online at http://www.pnas.org/lookup/suppl/doi:10.1073/pnas.2201249119/-/DCSupplemental.

Published July 25, 2022.

superoxide generation in nonphagocytes (10, 11), suggesting that the ligand concentration–dependent activation of phagocyte functions is regulated at the levels of agonist binding and transmembrane signaling.

Biased signaling has been seen in many GPCRs (12, 13). In published studies, agonists of GPCRs preferentially activate one signaling pathway over another, leading to different cellular activities. Therefore, biased signaling is a ligand-specific phenomenon in these reported cases. β-arrestins are frequent players in biased signaling. β-Arrestins are known for their roles in signal termination, GPCR endocytosis, and ERK activation (14). However, how FPR1 coupling to β-arrestins influences downstream pathways and activities is not fully understood, unlike for other GPCRs such as β-adrenergic receptors and angiotensin II receptors, with which different agonists preferentially activate the G protein pathway or the β-arrestin pathway (15, 16). It is well accepted that distinct receptor conformations are induced by different agonists that serve as determinants for the coupling of heterotrimeric G proteins versus β-arrestins (17). To understand how FPR1 selectively triggers signaling pathways when exposed to different concentrations of fMLF, we prepared a FlAsH-NanoBRET–based FPR1 biosensor for measurement of receptor conformational changes. We found that picomolar to subnanomolar concentrations of fMLF induced conformational changes that were consistent with the chemotaxis dose curve, whereas high nanomolar to micromolar concentrations of fMLF induced a different type of FPR1 conformation that matches the dose–response curves of degranulation and superoxide production. These results provide an example of ligand concentration–dependent signaling bias that may explain distinct phagocyte responses to various concentrations of chemoattractants.

Results

Distinct Phagocyte Functions Are Induced by Different Concentrations of fMLF. Dimethyl sulfoxide–differentiated HL-60 (dHL-60) cells that acquired neutrophil-like properties were stimulated with different concentrations of fMLF, and dose–response curves were generated using data collected from chemotaxis, degranulation, and superoxide production assays. As shown in Fig. 1*A*, chemotaxis was induced with subnanomolar concentrations of fMLF and peaked at 1 nM of the ligand (red curve). The chemotactic response gradually declined afterward and, at 100 nM, fMLF could no longer induce significant chemotaxis of dHL-60 cells. In contrast, degranulation (black curve) and superoxide production (blue curve) were not plateaued until the fMLF concentrations reached 1 μM. The same dose–response patterns were also observed in human peripheral blood neutrophils (Fig. 1*B*).

Correlation of Cytoplasmic Ca^{2+} Concentration Gradient with Chemotaxis, Degranulation, and Superoxide Production. Cytoplasmic Ca^{2+} concentration and distribution are closely associated with many cellular functions, including release of intracellular granules. To determine whether Ca^{2+} mobilization is associated with different cellular responses to fMLF, dHL-60 cells were loaded with a Ca^{2+}-sensitive fluorescent dye (FLIPR Calcium 5), and the fMLF-induced Ca^{2+} flux was measured in real time for the generation of dose–response curves (Fig. 1*C*). A rapid rise in cytoplasmic Ca^{2+} concentration was observed that plateaued after ∼20 s before a gradual decline. Treatment of the cells with pertussis toxin (PTX) abolished the fMLF-induced Ca^{2+} mobilization (blue line in Fig. 1*C*). Addition of ethylene glycol tetraacetic acid (EGTA), that chelates extracellular Ca^{2+}, markedly reduced the peak fluorescence as well as duration of Ca^{2+} mobilization (red line in Fig. 1*C* and blue line in Fig. 1*D*). These findings suggest that influx of extracellular Ca^{2+} could contribute to the rise in cytoplasmic Ca^{2+} concentration (18). Inclusion of EGTA in functional assays significantly reduced enzyme release (Fig. 1*E*) and superoxide production (Fig. 1*F*), suggesting that Ca^{2+} influx was required for these bactericidal functions of neutrophils.

Migration of granulocytes along a chemoattractant gradient may be accompanied by an cytoplasmic Ca^{2+} gradient (19). To determine whether fMLF at low and high concentrations could produce different effects on Ca^{2+} concentration gradient, dHL-60 cells were loaded with FLIPR Calcium 5 and stimulated with fMLF from 1 nM to 1 μM. Fluorescent images were taken every 15 s after placing fMLF in the upper left corner for agonist concentration gradient formation. As shown in *SI Appendix*, Fig. S1*A*, the cells stimulated with 1 nM fMLF began to form lamellipodia at 30 s and migrated toward the source of the chemoattractant between 30 and 60 s. The intracellular Ca^{2+} distribution was uneven, with a lower concentration of Ca^{2+} in the moving front than in the cell body. In contrast, the cells stimulated with 1 μM fMLF displayed surface adhesion as evidenced by a flattened shape and increased membrane ruffle in all directions (*SI Appendix*, Fig. S1*B*). There was a rapid and uniform increase in cytoplasmic Ca^{2+} concentration 30 to 45 s after agonist stimulation, but no net movement of the cells toward the source of chemoattractant was recorded between 30 and 60 s. These results suggest that Ca^{2+} influx triggered by rising intracellular Ca^{2+} concentration (20, 21) abolishes cytoplasmic Ca^{2+} concentration gradient and has a negative impact on chemotaxis.

In migrating cells, the protrusions in the moving front often have lower volumes than the cell bodies. To offset the effect of this difference that may affect the outcome of Ca^{2+} concentration measurement, ratiometric analysis was conducted with the Ca^{2+} indicators Fluo-4 AM (with increased fluorescent intensity when bound to Ca^{2+}) and Fura Red AM (with decreased fluorescent intensity when bound to Ca^{2+}). Addition of 1 nM fMLF to the cells loaded with the ratiometric Ca^{2+} indicators induced a Ca^{2+} concentration gradient along the axis from moving front to trailing edge, with higher Ca^{2+} concentrations in the cell body than at the front protrusion (Fig. 2*A*). Quantification of 30 representative cells found that the Fluo-4 intensity (Fig. 2*C*) and the Fluo-4/Fura Red ratio (Fig. 2*F*) increased from leading edge to tailing edge. In comparison, 1 μM fMLF induced a uniform increase in Fluo-4 fluorescence intensity and simultaneous decrease in Fura Red intensity (Fig. 2*D*). The increase in the Fluo-4/Fura Red ratio also showed a uniform pattern (Fig. 2*G*).

Distinct FPR1 Conformational Changes Are Induced by Low and High Concentrations of fMLF. Direct binding studies have shown that FPR1 displays two binding affinities for fMLF, suggesting the presence of a high-affinity site (equilibrium dissociation constant $K_d \sim 1$ nM) and a low affinity site ($K_d \sim 100$ nM) (22). It appears that the dissociation constants for the high- and low-affinity binding sites correspond to the concentrations of fMLF that induce maximal chemotaxis and that activate degranulation and superoxide generation, respectively. Based on this observation, we postulated that agonist occupation of the high-affinity site is responsible for chemotaxis, whereas agonist binding of the low-affinity site leads to degranulation and superoxide generation. We further postulated that fMLF occupation of different binding sites could induce different conformational changes of the receptor. To test these hypotheses, a fluorescent biosensor was prepared by fusion of a nanoluc protein (23) to the C terminus of FPR1 and with simultaneous insertion of a

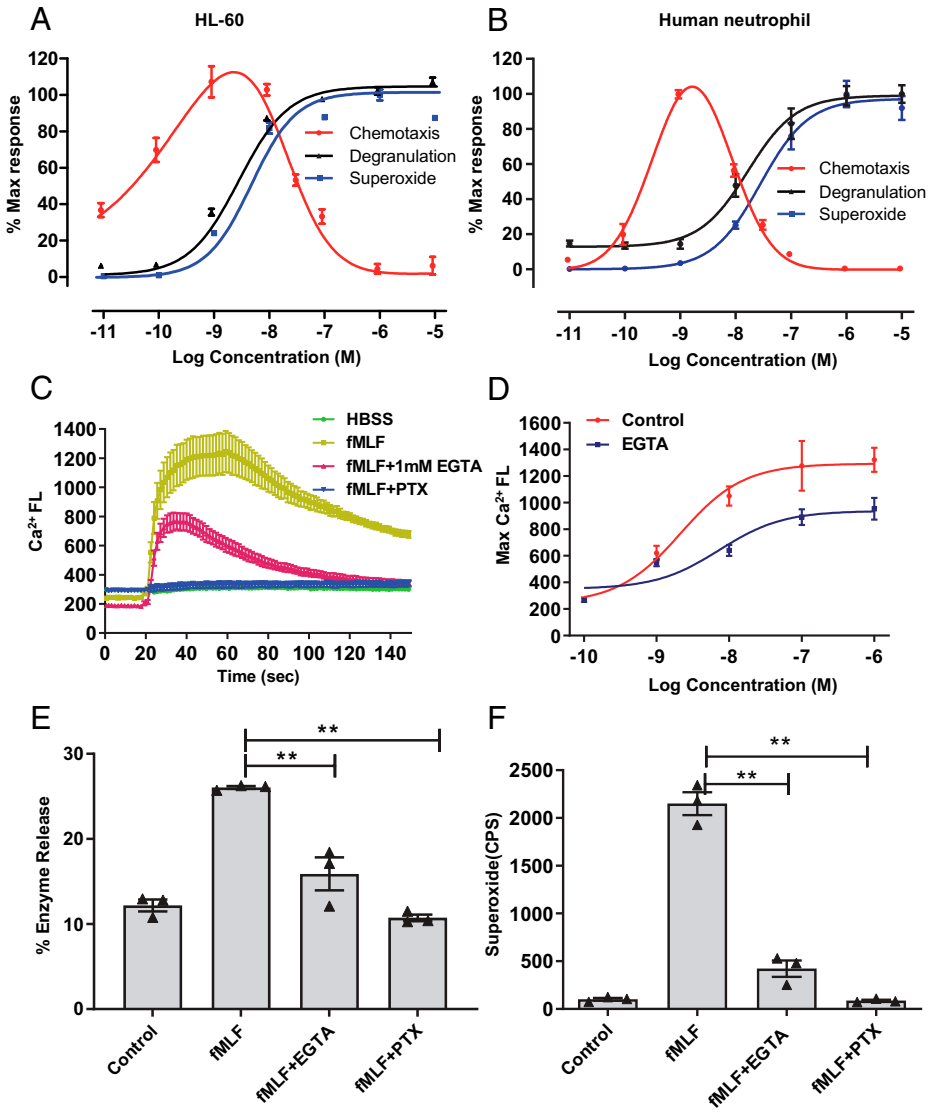

Fig. 1. Functions induced by fMLF at different concentrations. (*A* and *B*) The fMLF dose curves for chemotaxis, degranulation, and superoxide production were derived from stimulated dHL-60 cells (*A*) and peripheral blood neutrophils (*B*). Chemotaxis was conducted for 2 h at 37 °C and data were subject to checkerboard analysis. For degranulation, the cells were stimulated for 15 min at 37 °C, and the released β-hexosaminidase (*A*) and β-glucuronidase (*B*) were quantified. Superoxide production was measured in real time based on the chemiluminescence of isoluminol. (*C*) Effects of ethylene glycol tetraacetic acid (EGTA; 1 mM) and PTX (500 ng/mL, 6 h) on fMLF-induced Ca^{2+} mobilization. (*D*) Dose curves of Ca^{2+} flux in response to different concentrations of fMLF in the presence or absence of 1 mM EGTA. (*E* and *F*) The effects of PTX and EGTA on degranulation (*E*) and superoxide production (*F*) were also measured in dHL-60 cells stimulated with 1 μM fMLF. Data shown are means ± SEM from three independent experiments, each with triplicate measurements. $^{**}P < 0.01$. CPS, counts per second; FL, fluorescence intensity; Max, maximum.

FlAsH-binding motif (Cys-Cys-Pro-Gly-Cys-Cys) (24) into one of the intracellular loops (Fig. 3*A*). The agonist-induced conformational changes could be measured based on changes in the distance between the FlAsH-binding motif and the nanoluc, as reflected in the changes of the bioluminescence resonance energy transfer (BRET) intensity. This BRET-based biosensor, termed FPR1-IL3-Luc, retained receptor functions and was indistinguishable from the wild-type FPR1 in receptor internalization (Fig. 3*B*) and Ca^{2+} mobilization (Fig. 3*C*) assays. Stimulation with subnanomolar concentrations of fMLF (up to 1 nM) resulted in robust BRET between the inserted FlAsH binding motif and the nanoLuc (Fig. 3*D*), indicating shortening of the distance between the third intracellular loop and the C-terminal end with enhanced BRET. However, stimulation with fMLF at 10 nM or greater led to dose-dependent reduction in the BRET intensity (Fig. 3*D*), suggesting a different conformational change with increased distance between the third intracellular loop and the C terminus of FPR1. It is possible that fMLF at 10 nM or greater triggered the binding of a low-affinity site, thereby inducing different conformational changes of FPR1.

G proteins are both effectors and allosteric modulators of GPCRs (25, 26). G protein modulation of GPCR conformational states was elegantly shown in several studies using pharmacological tools (27, 28) and through structural analysis of GPCR–G protein complex (29, 30). To determine whether Gi coupling plays a role in the observed conformational switch of FPR1, the cells expressing the FPR1 biosensor were treated with PTX (500 ng/mL over 6 h) that uncouples the Gi protein from the receptor (8). PTX treatment reduced the BRET ratio by about 50% but did not affect the dose–response pattern that reflects FPR1 conformational changes in the fMLF concentration range tested (Fig. 3*E*).

Correlation between FPR1 Conformations and Signaling Pathways. The majority of GPCR functional assays were conducted at agonist concentrations ranging from 1 nM to 1 μM for

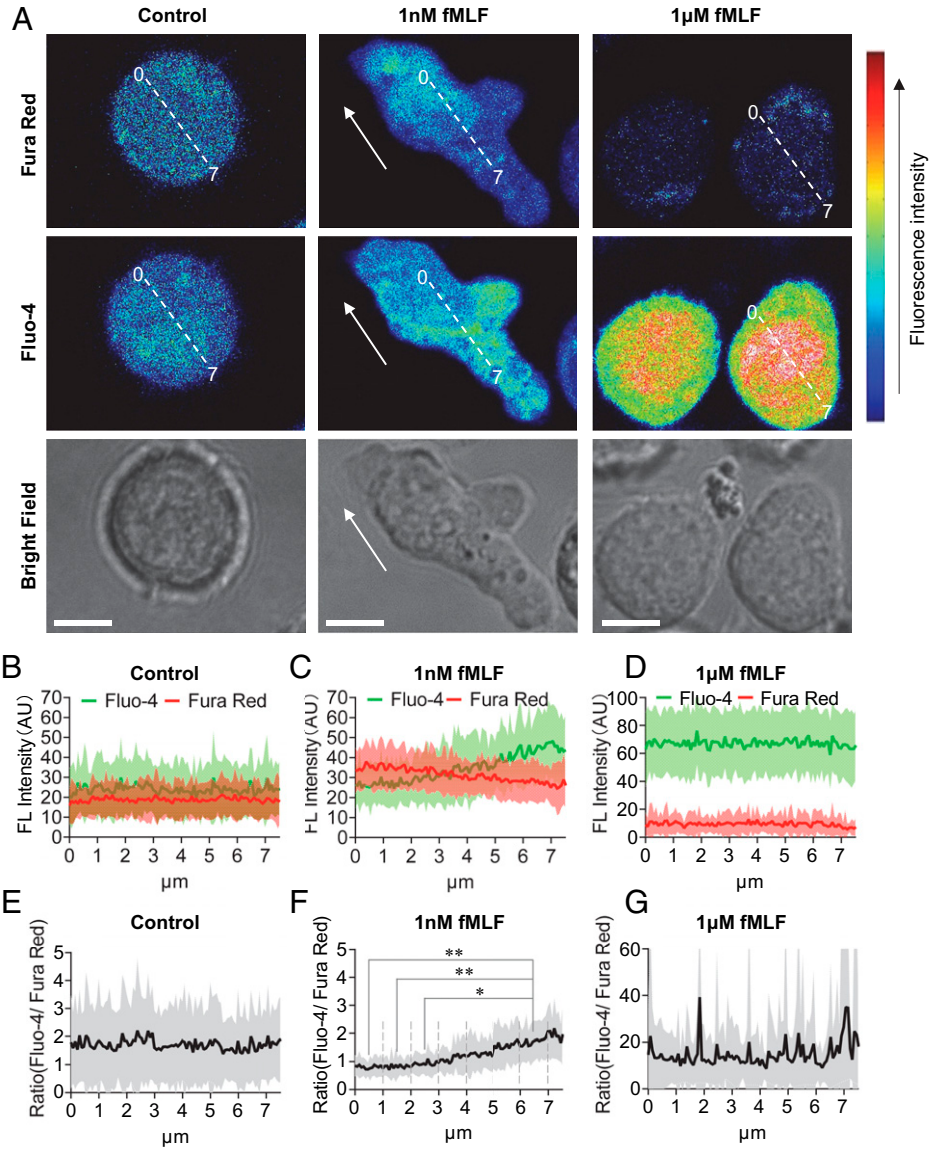

Fig. 2. fMLF-induced changes in cytoplasmic Ca^{2+} concentration. (*A*) dHL-60 cells were loaded with Fluo-4 AM and Fura Red AM for 1 h at 37 °C and treated with a point source of fMLF (1 nM and 1 μM, upper left corner of the viewing field). Arrows indicate direction of cell movement. Confocal microscopy images were taken from 30 cells and representative images are shown. (Scale bar, 5 μm.) (*B–D*) Fluorescence intensity (FL) of Fluo-4 (green lines) and Fura Red (red lines) was measured along the cell section (marked 0 to 7) and background fluorescence at each of the 92 data points was subtracted. (*B–D*) The processed data from control (*B*; no agonist), 1 nM fMLF (*C*), and 1 μM fMLF (*D*) were plotted. (*E–G*) Ratios of Fluo-4 to Fura Red from control (*E*; no agonist), 1 nM fMLF (*F*), and 1 μM fMLF (*G*) are plotted. Data are shown as means ± SEM based on 30 cells. (*F*) The average values collected from the first 3 μm were significantly lower than the average values in the last 1 μm, indicating lower cytoplasmic Ca^{2+} concentration in the leading edge of the migrating cells. $^{*}P < 0.05$, $^{**}P < 0.01$. AU, arbitrary units.

measurement of GPCR activities in vitro. We tested antibody arrays for fMLF-induced phosphorylation of 24 protein kinases (*SI Appendix*, Figs. S2 and S3). Two protein kinases, including ERK1/2 and RSK1, displayed prominent phosphorylation when dHL-60 cells were stimulated with fMLF at 1 nM or greater (*SI Appendix*, Fig. S2*A–C*). Western blotting analysis was conducted to verify the findings (*SI Appendix*, Fig. S2*D* and *E*). ERK1/2 have been known for their agonist-dependent phosphorylation up to 10 μM (31). Therefore, the phosphorylation profile matches that of the FPR1 conformation state induced by fMLF of 1 nM or greater, which is consistent with the established function of ERK1/2 as negative regulators of chemotaxis (31). Ribosomal protein S6 kinase 1 (RSK1, MAPKAPK1) is a protein kinase downstream of ERK1/2, and its phosphorylation was increased at 1 nM to 100 nM of fMLF and declined afterward (*SI Appendix*, Fig. S2*E*). Western blotting identified AKT phosphorylation starting with 1 nM fMLF stimulation, which plateaued at the fMLF concentration of 100 nM (*SI Appendix*, Fig. S2*F*).

β-Arrestins are multifunctional proteins that play an important role in GPCR signaling, desensitization, and internalization (32–34). To determine whether β-arrestins contributed to biased signaling in response to fMLF stimulation, HeLa cells were transfected to express mRuby2-tagged β-arrestin1 (β-Arr1) (Fig. 4*A*) or β-arrestin2 (β-Arr2) (Fig. 4*B*) together with FPR1, which was Clover tagged. The cells were then stimulated for 10 min with different concentrations of fMLF. Based on captured images, the intracellular β-Arr1 moved toward the nucleus and plasma membrane upon stimulation with 100 nM fMLF (Fig. 4*A*); in comparison, β-Arr2 translocated from the cytoplasmic milieu to the plasma membrane after fMLF (100 nM) stimulation (Fig. 4*B*). No significant translocation of β-arrestins was observed at fMLF concentrations of 10 nM or less. Quantification of the β-arrestin recruitment was conducted by cotransfecting a SmBiT-tagged

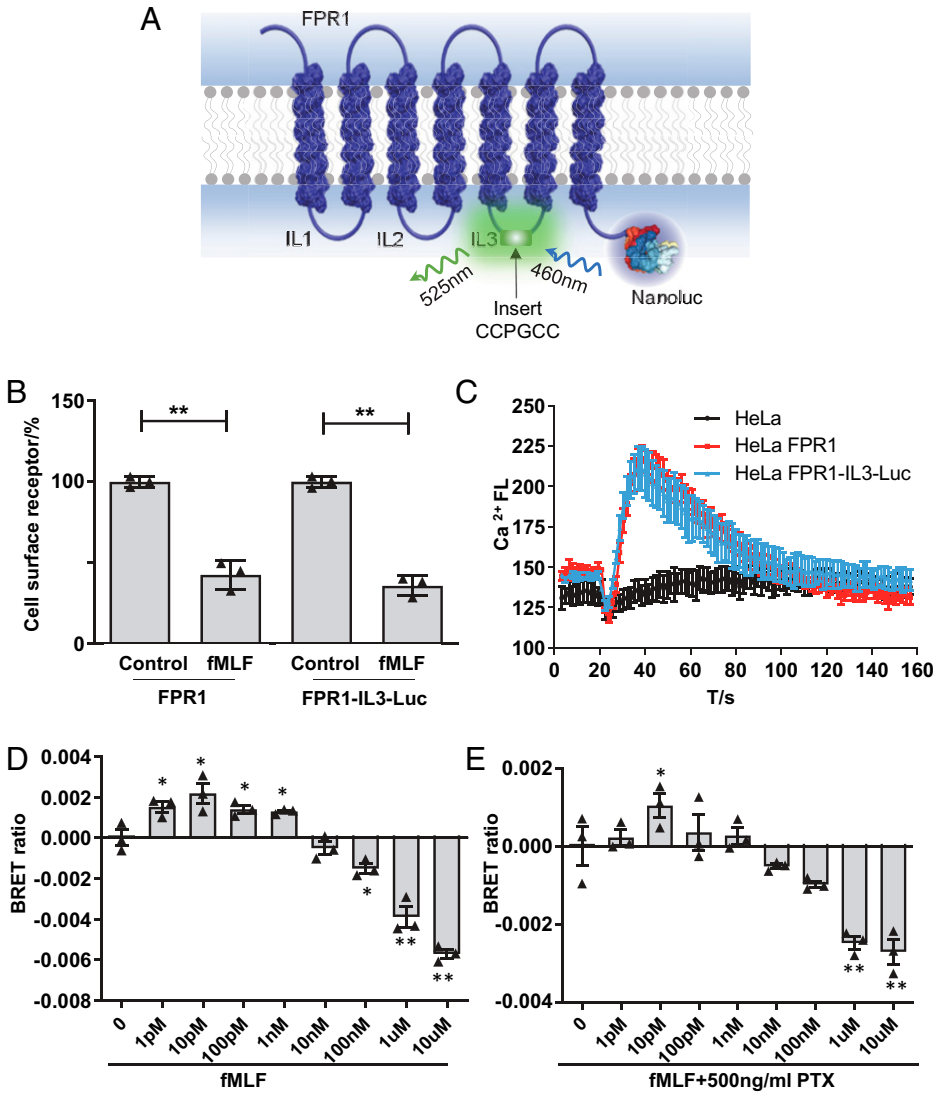

Fig. 3. Assessment of fMLF-induced conformational changes using a NanoBRET-based FPR1 biosensor. (*A*) Schematic representation of a FlAsH-NanoBRET–based FPR1 biosensor. The Nanoluc (donor) was fused to the C terminus of FPR1. A tetracysteine tag (CCPGCC) for FlAsH (acceptor) binding was inserted into the third intracellular loop (IL3) to form the biosensor, FPR1-IL3-Luc, which detects alterations in distance between the donor and the acceptor. (*B* and *C*) The functional integrity of the FPR1 biosensor was examined by fMLF (1 μM)-induced internalization (*B*) and Ca^{2+} mobilization (*C*), and was found to be indistinguishable from the wild-type FFP1. (*D* and *E*) Measurement of fMLF-induced conformational changes using the FPR1 biosensor. HeLa cells expressing FPR1-IL3-Luc were loaded with 1 μM FlAsH-EDT2 and then coelenterazine H (nanoluc substrate) was added to 5 μM for 5 min at 37 °C. BRET ratio was recorded for 100 s before and 100 s after stimulation in the presence of fMLF at different concentrations. In (*E*), PTX was added to 500 ng/mL and the cells were incubated for 6 h before fMLF treatment. The data shown are means ± SEM from 3 independent experiments, each measured in triplicate. **P* < 0.05, ***P* < 0.01.

FPR1 and LgBiT-tagged β-Arr1 or β-Arr2 (Fig. 4*C*). Membrane translocation of the tagged β-arrestins led to complementation of the small and large fragments of nanoluc protein, resulting in quantifiable luminescence. The results (Fig. 4*D*) are consistent with the image studies and together support FPR1-mediated β-arrestin recruitment at fMLF concentrations of 100 nM or greater. It is possible that as fMLF concentration increases, β-arrestin activation leads to desensitization of the receptor, thereby diminishing chemotaxis.

Discussion

In the present study, we investigated the mechanism by which fMLF at different concentrations induces distinct phagocyte functions. Our results indicate that subnanomolar concentrations of fMLF failed to stimulate Ca^{2+} mobilization but induced chemotaxis as well as conformational changes of the receptor FPR1. Of interest, increasing the concentrations of fMLF to the high nanomolar and micromolar range resulted in a different type of receptor conformational change, matching the fMLF concentrations required for degranulation and superoxide production. Accordingly, fMLF at these concentrations could induce Ca^{2+} influx and β-arrestin membrane translocation but suppress chemotaxis. Disruption of intracellular Ca^{2+} concentration gradient, induced activation of ERK1/2, and recruitment of β-arrestins are contributing factors to the suppression of chemotaxis.

These findings have led us to propose that chemotaxis is differentially regulated at the receptor level through a distinct receptor conformation induced by subnanomolar concentrations of fMLF. In contrast, higher concentrations of fMLF induce different conformational changes of FPR1, leading to Ca^{2+} mobilization and influx. Elevation of cytoplasmic Ca^{2+}, which is required for degranulation and superoxide generation, has a negative impact on chemotaxis. Our hypothesis challenges the established concept that a single G protein–coupling

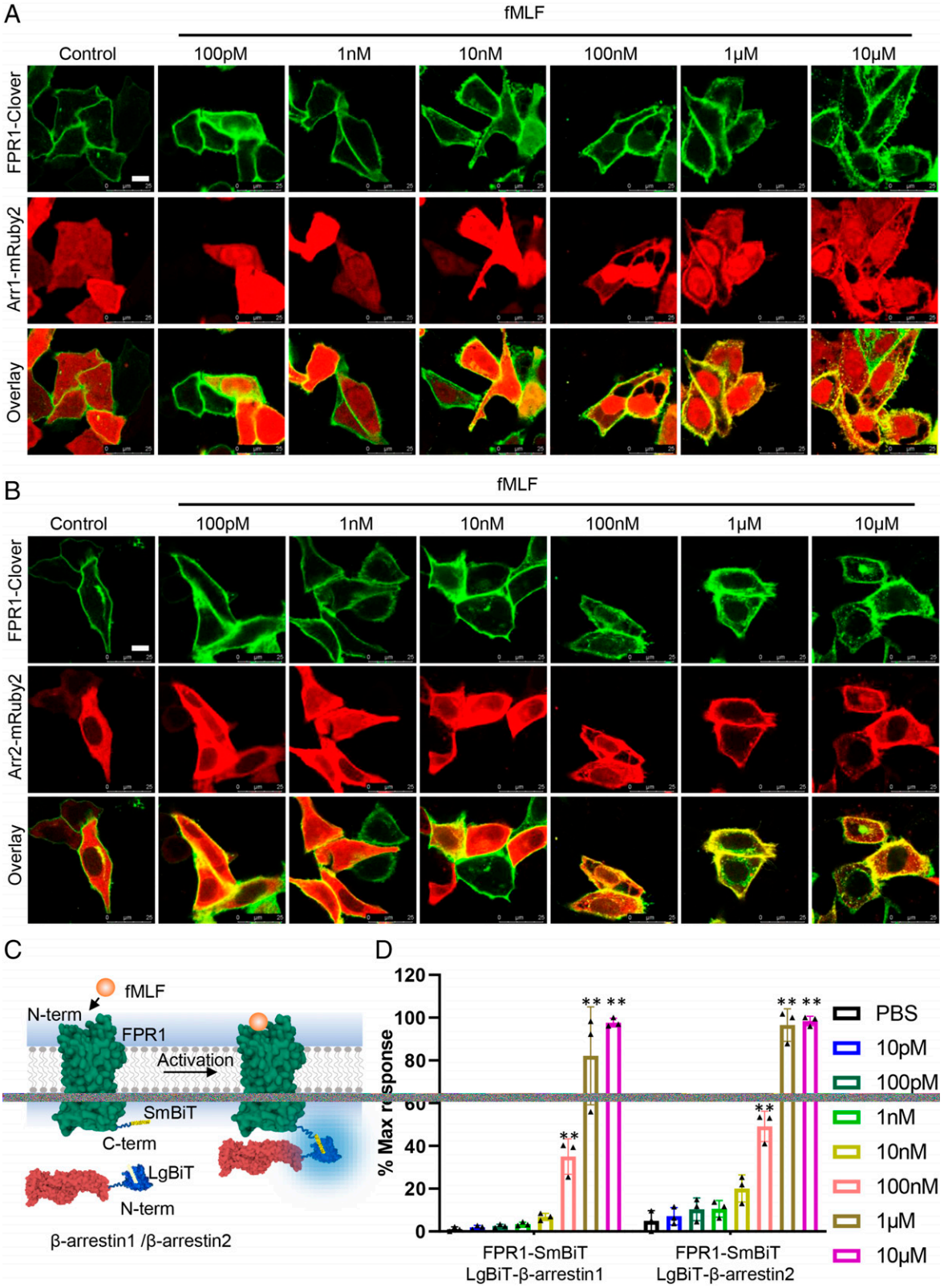

Fig. 4. Effect of different concentrations of fMLF on the recruitment of β-arr1 and β-arr2. (*A* and *B*) HeLa cells were cotransfected with FPR1-Clover (green fluorescence) and mRuby2-tagged β-arr1 (*A*) and β-arr2 (*B*). After 24 h, the cells were treated with different concentrations of fMLF for 10 min at 37 °C. Confocal microscopy images showing membrane translocation of the β-arrestins (red fluorescence) were taken and overlaid to show colocalization of these tagged proteins (yellow). The experiments were performed using a confocal microscope with a 40× oil objective, and representative pictures are shown. (Scale bar, 10 μm.) (*C*) schematic representation of a NanoBiT-based β-arrestin recruitment assay showing luminescence emission when the β-arrestin protein is recruited to FPR1 in the plasma membrane. (*D*) Quantification of FPR1-dependent recruitment of β-arr1 and β-arr2. HeLa cells cotransfected with FPR1-SmBiT and LgBiT–β-arrestins. Twenty-four hours after transfection, the substrate coelenterazine H (10 μM) was added and cells were incubated for 25 min at 37 °C before measurement of basal luminescence emission. The agonist fMLF was then added at the indicated concentrations and luminescence emission was measured again. Data (count per second) were plotted as a function of fMLF concentrations with the maximal luminescence emission (10 μM) set as 100% response. Data shown are mean ± SEM based on three independent experiments. Max, maximum; PBS, phosphate-buffered saline; term, terminus.

mechanism is responsible for chemotaxis, degranulation, and superoxide production (8). In support of this notion, a recent report on FPR2 activation showed that the aspirin-triggered lipoxins could induce FPR2 conformational changes at picomolar concentrations without stimulating measurable activities of the receptor (35). The induced FPR2 conformational change has been associated with the antiinflammatory activities of aspirin-triggered lipoxins (35).

The Ca^{2+} gradient was thought to play an important role in neutrophil migration. In polarized neutrophils, cytoplasmic Ca^{2+} concentration progressively decreases from the back (uropod) to the front (lamellipod) (*SI Appendix*, Fig. S1, and schematically depicted in *SI Appendix*, Fig. S4) (19, 36, 37). This Ca^{2+} concentration gradient was associated with persistent migration of polarized cells (38, 39). In the present study, a cytoplasmic Ca^{2+} concentration gradient was observed when dHL-60 cells were stimulated with subnanomolar concentrations of fMLF. In addition, elevation of cytoplasmic Ca^{2+} concentration may occur after integrin activation in adherent neutrophils and/or Fcγ receptor activation. Since no chemoattractant concentration gradient is associated with the integrins and Fcγ receptors, it is believed that the agonist-bound FPR1 at the leading edge of a polarized neutrophil is primarily responsible for the formation of the cytoplasmic Ca^{2+} concentration gradient. A subnanomolar concentration of fMLF may induce receptor conformation that is opposite to the one required for Gi protein activation, serving the function of an inverse agonist through elevation of the free-energy threshold for receptor activation. As a result, there is a localized decrease in cytoplasmic Ca^{2+} concentration at the leading edge of the polarized neutrophils, thus maintaining sustained cell migration (*SI Appendix*, Fig. S4).

When the cells are exposed to high concentrations of fMLF, the conformational change of FPR1 favors full activation of Gi proteins, leading to activation of PLCβ through the release of Gβγ subunits. The resulting production of diacyl glycerol and inositol 3,4,5-trisphosphate causes release of Ca^{2+} from intracellular stores, including the endoplasmic reticulum (18). This transient Ca^{2+} mobilization is followed by a sustained influx of Ca^{2+} from the extracellular milieu, where a higher Ca^{2+} concentration is present. The opening of the calcium-release activated Ca^{2+} channels Orai1 and Orai2 that are major components of these channels in neutrophils (40) leads to Ca^{2+} influx that is required for degranulation and superoxide generation. Likewise, the loss of stromal-interacting molecule 1 (that interacts with Orai1 for its activation; *SI Appendix*, Fig. S4) abrogated phagocyte NADPH oxidase activation and compromised bacterial killing (41). Meanwhile, Ca^{2+} influx abolishes the cytoplasmic Ca^{2+} gradient, thereby inhibiting chemotaxis. Consistent with this finding, it was reported that targeted deletion of the mouse gene coding for PLCβ2, a major form of PLCβ in neutrophils, enhanced chemotaxis of different leukocyte populations while compromising superoxide production and MAC-1 up-regulation in neutrophils (42). In addition, membrane translocation of β-arrestins in response to high concentrations of fMLF promotes desensitization of FPR1 and serves as a negative feedback mechanism. Consistent with this notion, targeted deletion of the *β-arr2* gene led to improved neutrophil recruitment in response to a chemokine (43).

Our investigation has led to the finding that subnanomolar and high nanomolar concentrations of fMLF could induce distinct conformational changes in FPR1. Since this phenomenon was observed in cells expressing only FPR1 but not other FPRs, it is probably caused by ligand binding to sites with different affinities. FPR1 contains binding sites with high and low affinities (22). Studies have shown that the high affinity site represents one that couples to heterotrimeric G proteins, and the low affinity site is uncoupled from the G proteins (7, 44). These studies were conducted with plasma membranes prepared from neutrophils that contained a subpopulation of FPR1 uncoupled from the Gi proteins. In the present study, FPR1 expressed in intact cells displayed different conformational changes in response to subnanomolar and high nanomolar concentrations of fMLF, and the agonist dose–response pattern was not altered by PTX treatment. These findings indicate that FPR1 conformational change induced by an agonist is an intrinsic property of the receptor. However, in PTX-treated cells, the BRET ratio was lower than in untreated cells, suggesting an allosteric effect of Gi proteins on FPR1 binding of the agonist fMLF (7, 44). It has been reported that fMLF binding to FPR1 may be regulated by not only Gi proteins but also by other cellular components such as actin (45).

In summary, using a BRET-based FPR1 biosensor, we identified ligand concentration–dependent changes in FPR1 conformations that correspond to selective activation of different phagocyte functions. An understanding of ligand concentration–dependent biased signaling may expand the scope of research on GPCR signaling and its physiological relevance. Further investigation of the mechanisms for neutrophil chemotaxis will require the correlation of the low-fMLF–induced FPR1 conformation with signaling events occurring in a polarized cell, in which the distribution of signaling molecules is key to the direction of cell movement.

Materials and Methods

Materials. The sources of reagents for cell culture and transfection, chemotaxis, degranulation, superoxide production, calcium concentration measurement, and BRET analysis are described in *SI Appendix, Materials and Methods*.

Cells. Human promyelocytic HL-60 cells were differentiated with dimethyl sulfoxide (1.3%) for 5 d. Human neutrophils from peripheral blood were prepared by density-gradient centrifugation using institutional approved protocols. Details of cell culture and preparation are provided in *SI Appendix, Materials and Methods*.

Plasmids. Modifications of complementary DNAs for FPR1, β-Arr1 and β-Arr2 were carried out by PCR, using the complementary DNA of NanoLuc derivatives and fluorescent proteins for fusion protein construction. The final products including the FPR1 biosensors were subcloned into the expression vector pCDNA3.1. For details, please refer to *SI Appendix, Materials and Methods*.

Chemotaxis, Degranulation, and Superoxide Production. These established neutrophil functional assays were carried out using Transwell (chemotaxis), β-glucuronidase and β-hexosaminidase determination (degranulation), and the isoluminol method (superoxide production). Detailed protocols are provided in *SI Appendix, Materials and Methods* sections.

Calcium Concentration Measurements. Calcium flux was determined using the FLIPR Calcium 5 reagents as described in *SI Appendix, Materials and Methods*. Live cell imaging of Ca^{2+} concentration gradient was carried out first using FLIPR Calcium 5 and then using the ratiometric Ca^{2+} indicators Fluo-4 AM and Fura Red AM. These experiments are described in detail in *SI Appendix, Materials and Methods*.

β-Arrestin Recruitment. Two sets of experiments were conducted. First, MRuby2-tagged β-Arr1 and β-Arr2 were cotransfected with Clover-tagged FPR1, and colocalization of β-arrestins and FPR1 was determined by fluorescent confocal microscopy. Second, NanoBiT constructs were prepared for NanoLuc complementation between SmBiT-tagged FPR1 and LgBiT-tagged β-arrestins. For experimental details, please refer to *SI Appendix, Materials and Methods*.

BRET Measurement. An FPR1 biosensor was engineered to contain a FlAsH-binding motif in its intracellular loops and NanoLuc in its C terminus. BRET was measured after stimulation of the FPR1 biosensor with different concentrations of fMLF. The detailed procedures of biosensor construction and BRET measurements are presented in *SI Appendix, Materials and Methods*.

Phosphorylation of Signaling Molecules. Human phosphor-MAPK array was used for determination of FPR1 signaling events, and changes detected were verified by Western blotting. Detained information can be found in *SI Appendix, Materials and Methods*.

Data Availability. All study data are included in the article and/or *SI Appendix* and will be accessible upon publication.

ACKNOWLEDGMENTS. We thank Ms. Yixin Chang and Ms. Congcong Xu for their guidance in neutrophil preparation. This work was supported in part by the National Key R&D Program of China (Grant 2019YFA0906003), Shenzhen Bay Laboratory Open Project (Grant SZBL2020090501011), Shenzhen Natural Science Foundation Project (Grant GXWD20201231105722002-20200831175432002) and the 70th batch of General Projects from China Postdoctoral Science Foundation (Grant 2021M703092).

1. R. D. Ye *et al.*, International Union of Basic and Clinical Pharmacology. LXXIII. Nomenclature for the formyl peptide receptor (FPR) family. *Pharmacol. Rev.* **61**, 119–161 (2009).
2. F. Boulay, M. Tardif, L. Brouchon, P. Vignais, The human *N*-formylpeptide receptor. Characterization of two cDNA isolates and evidence for a new subfamily of G-protein-coupled receptors. *Biochemistry* **29**, 11123–11133 (1990).
3. W. A. Marasco *et al.*, Purification and identification of formyl-methionyl-leucyl-phenylalanine as the major peptide neutrophil chemotactic factor produced by *Escherichia coli*. *J. Biol. Chem.* **259**, 5430–5439 (1984).
4. C. Nathan, Neutrophils and immunity: Challenges and opportunities. *Nat. Rev. Immunol.* **6**, 173–182 (2006).
5. E. Kolaczkowska, P. Kubes, Neutrophil recruitment and function in health and inflammation. *Nat. Rev. Immunol.* **13**, 159–175 (2013).
6. N. Chiang, C. N. Serhan, Specialized pro-resolving mediator network: An update on production and actions. *Essays Biochem.* **64**, 443–462 (2020).
7. C. Koo, R. J. Lefkowitz, R. Snyderman, The oligopeptide chemotactic factor receptor on human polymorphonuclear leukocyte membranes exists in two affinity states. *Biochem. Biophys. Res. Commun.* **106**, 442–449 (1982).
8. G. M. Bokoch, A. G. Gilman, Inhibition of receptor-mediated release of arachidonic acid by pertussis toxin. *Cell* **39**, 301–308 (1984).
9. W. M. Nauseef, N. Borregaard, Neutrophils at work. *Nat. Immunol.* **15**, 602–611 (2014).
10. M. Nanamori, J. Chen, X. Du, R. D. Ye, Regulation of leukocyte degranulation by cGMP-dependent protein kinase and phosphoinositide 3-kinase: Potential roles in phosphorylation of target membrane SNARE complex proteins in rat mast cells. *J. Immunol.* **178**, 416–427 (2007).
11. B. Nie, N. Cheng, M. C. Dinauer, R. D. Ye, Characterization of P-Rex1 for its role in fMet-Leu-Phe-induced superoxide production in reconstituted COS(phox) cells. *Cell. Signal.* **22**, 770–782 (2010).
12. C. M. Costa-Neto, L. T. Parreiras-E-Silva, M. Bouvier, A pluridimensional view of biased agonism. *Mol. Pharmacol.* **90**, 587–595 (2016).
13. J. W. Wisler, H. A. Rockman, R. J. Lefkowitz, G. Biased, Biased G protein-coupled receptor signaling: Changing the paradigm of drug discovery. *Circulation* **137**, 2315–2317 (2018).
14. A. K. Shukla, K. Xiao, R. J. Lefkowitz, Emerging paradigms of β-arrestin-dependent seven transmembrane receptor signaling. *Trends Biochem. Sci.* **36**, 457–469 (2011).
15. D. S. Kang, X. Tian, J. L. Benovic, Role of β-arrestins and arrestin domain-containing proteins in G protein-coupled receptor trafficking. *Curr. Opin. Cell Biol.* **27**, 63–71 (2014).
16. L. M. Wingler *et al.*, Angiotensin and biased analogs induce structurally distinct active conformations within a GPCR. *Science* **367**, 888–892 (2020).
17. L. M. Wingler, R. J. Lefkowitz, Conformational basis of G protein-coupled receptor signaling versatility. *Trends Cell Biol.* **30**, 736–747 (2020).
18. M. J. Berridge, The inositol trisphosphate/calcium signaling pathway in health and disease. *Physiol. Rev.* **96**, 1261–1296 (2016).
19. R. A. Brundage, K. E. Fogarty, R. A. Tuft, F. S. Fay, Calcium gradients underlying polarization and chemotaxis of eosinophils. *Science* **254**, 703–706 (1991).
20. M. J. Berridge, Inositol trisphosphate and calcium signalling. *Nature* **361**, 315–325 (1993).
21. C. C. Petersen, O. H. Petersen, M. J. Berridge, The role of endoplasmic reticulum calcium pumps during cytosolic calcium spiking in pancreatic acinar cells. *J. Biol. Chem.* **268**, 22262–22264 (1993).
22. R. D. Ye *et al.*, The rabbit neutrophil *N*-formyl peptide receptor. cDNA cloning, expression, and structure/function implications. *J. Immunol.* **150**, 1383–1394 (1993).
23. C. G. England, E. B. Ehlerding, W. Cai, NanoLuc: A small luciferase is brightening up the field of bioluminescence. *Bioconjug. Chem.* **27**, 1175–1187 (2016).
24. S. R. Adams *et al.*, New biarsenical ligands and tetracysteine motifs for protein labeling in vitro and in vivo: Synthesis and biological applications. *J. Am. Chem. Soc.* **124**, 6063–6076 (2002).
25. B. T. DeVree *et al.*, Allosteric coupling from G protein to the agonist-binding pocket in GPCRs. *Nature* **535**, 182–186 (2016).
26. X. Sun, S. Singh, K. J. Blumer, G. R. Bowman, Simulation of spontaneous G protein activation reveals a new intermediate driving GDP unbinding. *eLife* **7**, e38465 (2018).
27. S. Mary *et al.*, Ligands and signaling proteins govern the conformational landscape explored by a G protein-coupled receptor. *Proc. Natl. Acad. Sci. U.S.A.* **109**, 8304–8309 (2012).
28. J. Cabana *et al.*, Identification of distinct conformations of the angiotensin-II type 1 receptor associated with the Gq/11 protein pathway and the β-arrestin pathway using molecular dynamics simulations. *J. Biol. Chem.* **290**, 15835–15854 (2015).
29. S. G. Rasmussen *et al.*, Crystal structure of the β2 adrenergic receptor-Gs protein complex. *Nature* **477**, 549–555 (2011).
30. C. J. Tsai *et al.*, Crystal structure of rhodopsin in complex with a mini-G_o sheds light on the principles of G protein selectivity. *Sci. Adv.* **4**, eaat7052 (2018).
31. X. Liu *et al.*, Bidirectional regulation of neutrophil migration by mitogen-activated protein kinases. *Nat. Immunol.* **13**, 457–464 (2012).
32. S. S. Ferguson *et al.*, Role of beta-arrestin in mediating agonist-promoted G protein-coupled receptor internalization. *Science* **271**, 363–366 (1996).
33. Y. K. Peterson, L. M. Luttrell, The diverse roles of arrestin scaffolds in G protein-coupled receptor signaling. *Pharmacol. Rev.* **69**, 256–297 (2017).
34. J. van Gastel *et al.*, β-Arrestin based receptor signaling paradigms: Potential therapeutic targets for complex age-related disorders. *Front. Pharmacol.* **9**, 1369 (2018).
35. Y. Ge *et al.*, Dual modulation of formyl peptide receptor 2 by aspirin-triggered lipoxin contributes to its anti-inflammatory activity. *FASEB J.* **34**, 6920–6933 (2020).
36. R. A. Brundage, K. E. Fogarty, R. A. Tuft, F. S. Fay, Chemotaxis of newt eosinophils: Calcium regulation of chemotactic response. *Am. J. Physiol.* **265**, C1527–C1543 (1993).
37. F. C. Tsai *et al.*, A polarized Ca2+, diacylglycerol and STIM1 signalling system regulates directed cell migration. *Nat. Cell Biol.* **16**, 133–144 (2014).
38. C. Wei *et al.*, Calcium flickers steer cell migration. *Nature* **457**, 901–905 (2009).
39. F. C. Tsai, G. H. Kuo, S. W. Chang, P. J. Tsai, Ca^{2+} signaling in cytoskeletal reorganization, cell migration, and cancer metastasis. *BioMed Res. Int.* **2015**, 409245 (2015).
40. D. Grimes *et al.*, ORAI1 and ORAI2 modulate murine neutrophil calcium signaling, cellular activation, and host defense. *Proc. Natl. Acad. Sci. U.S.A.* **117**, 24403–24414 (2020).
41. H. Zhang *et al.*, STIM1 calcium sensor is required for activation of the phagocyte oxidase during inflammation and host defense. *Blood* **123**, 2238–2249 (2014).
42. H. Jiang *et al.*, Roles of phospholipase C beta2 in chemoattractant-elicited responses. *Proc. Natl. Acad. Sci. U.S.A.* **94**, 7971–7975 (1997).
43. Y. Su *et al.*, Altered CXCR2 signaling in beta-arrestin-2-deficient mouse models. *J. Immunol.* **175**, 5396–5402 (2005).
44. C. Koo, R. J. Lefkowitz, R. Snyderman, Guanine nucleotides modulate the binding affinity of the oligopeptide chemoattractant receptor on human polymorphonuclear leukocytes. *J. Clin. Invest.* **72**, 748–753 (1983).
45. A. J. Jesaitis, R. W. Erickson, K. N. Klotz, R. K. Bommakanti, D. W. Siemsen, Functional molecular complexes of human *N*-formyl chemoattractant receptors and actin. *J. Immunol.* **151**, 5653–5665 (1993).